RESEARCH ARTICLE

Characterization of wettability effects on pressure drop of two-phase flow in microchannel

Prakash Rapolu · Sang Young Son

Abstract The Characterization of the effects of surface wettability and geometry on pressure drop of slug flow in isothermal horizontal microchannels is investigated for circular and square channels with hydraulic diameter (D_h) of 700 μm. Flow visualization is employed to characterize the bubble in slug flow established in microchannels of various surface wettabilities. Pressure drop increases with decrease in surface wettability, while the channel geometry influences slug frequency. It is observed that the gas–liquid contact line in advancing and receding interfaces of bubble change with surface wettability in slug flows. Flow resistance, where capillary force is important, is estimated using Laplace–Young equation considering the change of dynamic contact angles of bubble. The experimental study also demonstrates that the liquid film presence elucidates the pressure drop variation of slug flows at various surface wettabilities due to diminishing capillary effect.

1 Introduction

Micro- or mini- power and thermal management systems are used in the interest of providing higher performance capabilities besides being compact. Some of these applications involve gas–liquid two-phase flow in channels much less than 1 mm in diameter. Two-phase flow in microchannels is used ever increasingly in many wide ranging applications and is currently a very active research area. As the compactness increases possibly a higher pressure drop is observed in micro- or mini-flow channels.

P. Rapolu · S. Y. Son (✉)
Mechanical Engineering, School of Dynamic System,
University of Cincinnati, Cincinnati, OH 45221, USA
e-mail: sangyoung.son@uc.edu

Unlike in large scale systems, gas bubbles can present significant problems in microfluidic systems by disturbing and eventually blocking the flow. As surface area to volume ratio is very high for microchannels, surface forces become predominant over body forces for microscale applications. Gas–liquid interface behavior in a microchannel is more transient and complex than single-phase flow and creates many problems related to high surface tension and wetting effects (Ichikawa et al. 2005). Interactions on the boundaries between gas, liquid, and solid introduce nonlinearity and instabilities (Cubaud and Ho 2004).

Understanding how surface wettability and geometry of microchannels affect bubbles and in-turn flow resistance is a concern of design and process control of these microfluidic devices. For annular films without an imposed axial flow and no surface shear, it has been observed that the liquid will accumulate into lobes and, if the volume of liquid is sufficient, into lenticular lenses, or liquid plugs, which "pinch-off" the core flow. The formation of a lenticular lens from the liquid in the annular film is also referred to as "snap-off" or "liquid hold-up". Whether the adjacent lobes/lenses are connected to one another by a liquid film depends upon the flow rate as well as channel geometry. And the stability of the liquid film can significantly influence the inertia of the system through the morphological change from thin film to plug. The pinch-off results from a capillary-driven instability; commonly referred to as Rayleigh instability. Many fundamental studies on two-phase flow have confirmed the importance of the dynamics and stability of liquid films on the behavior of two-phase flow. Hence, it is critical to include the physics of the liquid film stability, where phase interaction is a combination of viscous and capillary effects, in scale modeling in order to properly characterize two-phase flow in microchannels.

Suo and Griffith ([1964](#)) performed studies of two-phase flow in capillaries. They concluded that since capillary slug flow exists in both horizontal and vertical tubes, the surface tension forces dominate over the gravity forces. Damianides and Westwater ([1988](#)) studied two-phase flow in tubes ranging from 1 to 5 mm. They concluded that the surface tension between the gas and liquid is a very important variable for two-phase flow in air–water systems with Pyrex glass tube diameters of ≤5 mm. Graska ([1986](#)), using liquids with different surface tensions, concluded that the liquid–gas surface tension is a significant variable in two-phase flow through Pyrex glass tubes with ID ≤ 5 mm. Barajas and Panton ([1994](#)) studied the effects of varied contact angle on the flow in 1.6-mm circular tube and concluded it is an important parameter affecting two-phase flow in capillaries.

Evident from the above studies surface forces become predominant over other body forces at microscale level. Given that static contact angle (θ_s) of liquid (characteristic signature of surface energy) influences the motion of the interface; characteristics of two-phase flow at microscale were bound to vary from those observed in common microchannels. Son and Allen ([2003](#)) visualized the effect of wettability on microchannel two-phase flow resistance. They illustrated that uncoated microchannels (hydrophilic in nature) show stable flow with high velocity liquid slugs translating on an annular liquid film while a commercial polymer-coated microchannel (hydrophobic in nature) exhibits less stable flow with droplet formation and contact line drag.

Very few experimental studies (Son and Allen [2004](#)) are available reporting the effect of geometry and contact angle (surface wettability) for same fluid two-phase flow in microchannels less than 1 mm. The experimental studies were carried out by Lee and Lee ([2008a](#), [b](#)) to ascertain influence of surface tension on flow characteristics by considering fluids of different surface energy. As we aim to increase our understanding of air–water two-phase flow, surface wettability of various size geometric microchannels is modified in this study.

This paper is organized as follows: In this present work, we aim to provide data allowing understanding the role of the surface wettability on the two-phase flow characteristics in microchannels with the hydraulic diameter as of

700 μm. Two-phase slug flow was established for various liquid volumetric fractions. We first discuss the effects of surface wettability on two-phase flow resistance followed by effects of geometry.

2 Experimental setup and procedure

Test setup consists of the visualization system, water and dry air supplying lines, and the differential pressure measurement setup. The volume flow rates of the single-phase flows (water and air) is inversely calculated using the laminar flow theory by measuring the frictional pressure drop across the single glass circular tube (Inside diameter = 1,095 μm and Length 95.25 mm) implemented in the single-phase supply lines (Fig. [1](#)). A high spatial resolution scientific CCD camera (1,024 × 768 pixels, 1/3-type progressive scanning, 10 bit depth, 1/20,000 shutter speed, 30 fps) captures the flow images through Nikon SMZ-800 stereo microscope.

2.1 Surface wettability modification

In order to study air–water two-phase flows on various surface wettability configurations, microchannel surface energy needs to be modified suitably. Chemical modification method is employed in this study to create the wall surfaces with various surface wettabilities with high optical transparency.

We carried out the thin film coatings of the microchannels by sol–gel dip coating methods so as to obtain transparent surfaces of superhydrophilic with the static contact angle (θ_s) as of 25° (Tadanaga et al. [2000](#)), hydrophobic and superhydrophobic as $\theta_s = 105°$ and $\theta_s = 150°$, respectively (Jeong et al. [2001](#)). For the hydrophilic surface wettability, the plain microchannels were used giving the static contact angle (θ_s) of 60°. As direct measurement of the contact angle inside the microchannel is not available, a reference section of cover glass surface is dip-coated simultaneously with the microchannels. Then, static contact angles of coated cover glass surfaces were measured using sessile-drop method by a surface analysis system (AST VCA Optima XE). The system uses automated gray-scale imaging and performs a droplet

Fig. 1 Schematic representation of the experimental set up to measure the pressure drop and to visualize the slug flow in microchannels
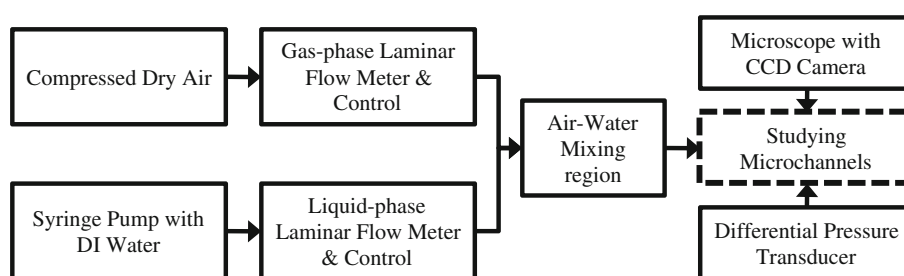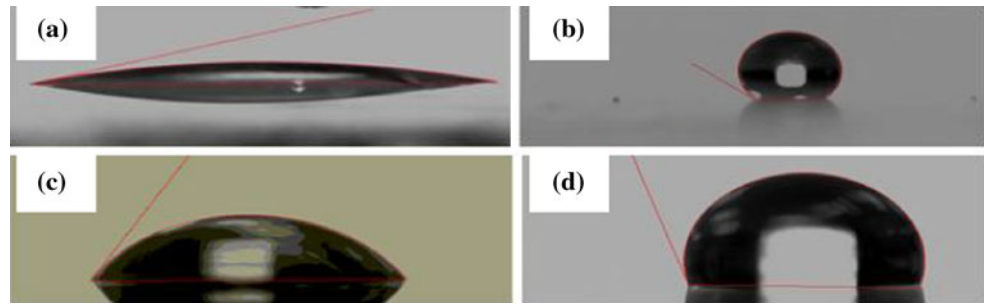
Fig. 2 Static contact angle measurements of various wettability surfaces: **a** Superhydrophilic ($\theta_s = 20°$), **b** Superhydrophobic ($\theta_s = 135°$), **c** Hydrophilic glass ($\theta_s = 60°$), and **d** Hydrophobic ($\theta_s = 105°$)

curve-fit and base-line determination to calculate the contact angle. Two microliters of DI water is dispensed into needle from gas-tight 100 µL syringe, using a syringe control on Optima software. The glass slide substrate is raised slowly until it touches water droplet. After water droplet settles on the glass substrate, it is retraced slowly and image of water droplet on surface is captured after 5 s. Mean static contact angle is computed using average of measurements (Fig. 2).

To ascertain stability of coated thin film surfaces on continuous presence in air and water, contact angles of coated sample substrates were measured over a period of time up to 30 days. Figure 3 illustrates static contact angle values of water on sample-coated surfaces. Static contact angle remained within measurement uncertainty of $\pm 2°$ over the 30-day time period.

2.2 Apparatus and procedure

Figure 1 illustrates experimental layout for the measurement of pressure drop and microscale flow visualization. A syringe pump (Harvard PHD 2000) infused de-ionized distilled water at Q_L (water volume flow rate) while dry air was supplied by regulating air cylinder supply at Q_G (dry air volume flow rate), which are inversely calculated using laminar flow theory by measuring frictional pressure drops across microchannels.

The experimental test microchannel sections were primarily of two different geometries of transparent wettability conditions from superhydrophilic to superhydrophobic. The control of flow regime is critical to the experiments and it is probable that some of the discrepancy in microscale two-phase flow data among various research groups results from insufficient isolation of entrance effects on the flow behavior (Allen and Son 2007). The two-phases (water and air) meet at the entrance region and naturally generate converging nozzle type entrance flow shown along with image in Fig. 4. In order to measure the pressure as well as supplying water, the plastic T-connector is used both for inlet and outlet of microchannel. The gap between T-connector and microchannel is self-sealed by thermally melting and compression of the plastic body of T-connector. Two thermocouples were used to measure the temperature of the ambient air near and
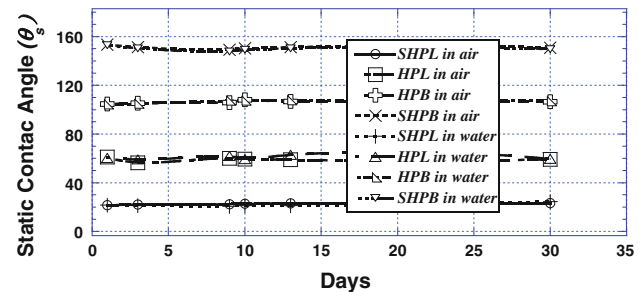

Fig. 3 Variation of static contact angle of coated surfaces with time in air and water; (*SHPL* superhydrophilic, *HPL* hydrophilic, *HPB* hydrophobic, and *SHPB* superhydrophobic)

away from the test section to verify isothermal conditions (Son and Allen 2005).

The flow regime of the two-phase flow is confirmed with the visualization of the flow patterns, recorded by the high resolution, high shutter speed CCD camera mounted on stereo microscope. The testing field of microchannel was illuminated by gooseneck fiber optic guides connected to two independent 150 and 250 W cold cathode quartz halogen fiber optic illuminators. Gooseneck guides were used to minimize heat input to the fluids due to illumination for isothermal condition. To record enlarged images of the two-phase flow inside the microchannel, a microscope objective lens (0.5×) coupled to video camera was used. Synchronized image and data acquisition are carried out by LabVIEW program.

Laminar theory is used to estimate the volume flow rate of single-phase fluid flows from pressure drop measurement using the differential pressure transducer (Druck EEx ia IICT4) in Fig. 1. The corresponding Reynolds numbers in the experimental conditions are found less than 25 and 230 for water and dry air flows, respectively. All pressure transducers had a differential pressure range of 34.5 kPa and are calibrated using pressure calibration system. The pressure drops in microchannel test section reached up to 12 kPa (75% of maximum load of pressure transducer). The transducer is checked for its initial value of 4 mA current output prior to running the test and confirmed following each test. Uncertainty in pressure measurement is $\pm 0.25\%$ of the maximum reading (i.e., ± 250 Pa).

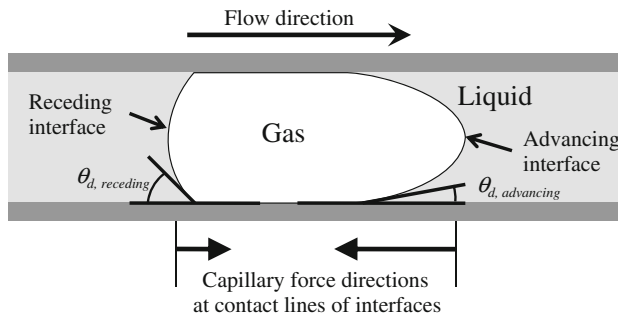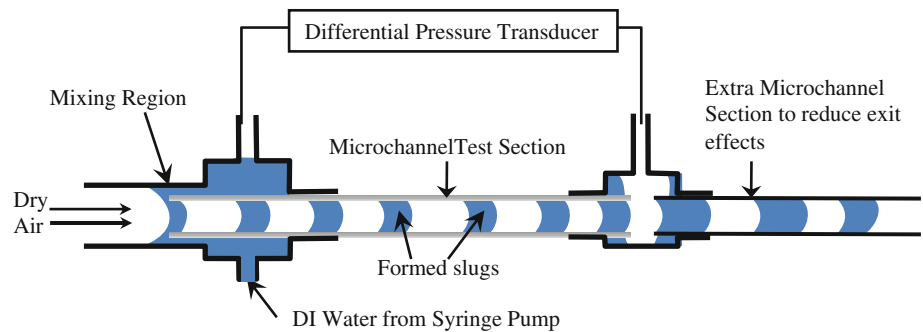**Fig. 4** Two-phase mixing region of microchannel slug flow experiment (Son and Allen 2005)

Fig. 5 Schematic representation of microchannel slug flow and dynamic contact angles at advancing and receding interfaces of single bubble
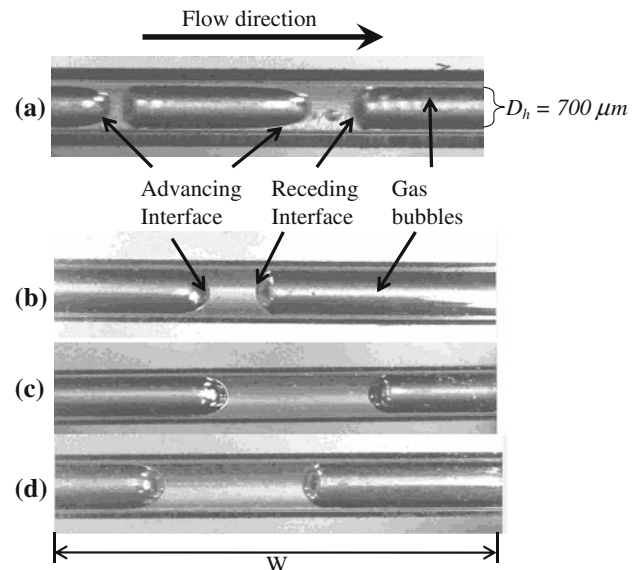

Fig. 6 Slug flows in 700-µm hydraulic-diamter circular microchannels of various wettabilities at α_L of 0.028 ($Q_L = 4.6 \times 10^{-8}$ m³/s and $Q_G = 1.6 \times 10^{-6}$ m³/s); **a** Superhydrophobic, **b** Hydrophobic, **c** Hydrophilic, and **d** Superhydrophilic walls. The width (W) of above channels is 2.1 mm that is equivalent to 512 pixels of CCD

3 Results and discussion

3.1 Dynamic contact angle versus surface wettability

Two-phase flows are distributed into several distinct flow patterns depending on gas and liquid volume flow rates and channel geometry. Only slug flow, which is commonly encountered in microchannel applications, is studied. Transitions between regimes are predicted as a function of liquid and gas flow rates. For both circular and square channels, transitions between each regime occur for fixed values of the liquid volumetric fraction α_L defined as

$$\alpha_L = Q_L / (Q_L + Q_G) \tag{1}$$

where Q_L and Q_G are the liquid and gas volume flow rates, respectively. Over the range of liquid volumetric flow rates investigated (α_L: 0.007–0.028), slug flow is observed in both geometric channels in this study. This case is different from the case of macrochannels and minichannels where differences in the relative effects of gravitational, shear, and surface tension forces cause the transitions to be dependent on the channel diameter (Bi and Zhao 2001).

Figure 5 schematically illustrates the dynamic contact angles (θ_d) at the advancing and receding fronts of a bubble in slug flow. The dynamic contact angle can be separated as advancing and receding depending on flow direction. Advancing and receding dynamic contact angles ($\theta_{d,\text{advancing}}$ and $\theta_{d,\text{receding}}$) are formed at the contact lines of front and

back interfaces, respectively. Due to the small hydraulic diameter of microchannel, the bubble (gas phase) occupies the whole cross-section of channel. The bubble deforms due to the capillary force formed at the advancing and receding interfaces in the pressure-driven slug flow. The degree of bubble deformation is governed by capillary force which is varied depending on surface wettability and channel geometry. Figure 6 indicates the snapshots of slugs for each wettability configuration for a liquid volumetric fraction, α_L of 0.028 corresponding to $Q_L = 4.6 \times 10^{-8}$ m³/s and $Q_G = 1.65 \times 10^{-6}$ m³/s. If there is no flow in the channel, the bubble may stay without its deformation. The corresponding contact angles at advancing and receding fronts may be identical to each other because there is no difference in capillary stress induced by flow.

For each slug flows shown in Fig. 6, the images are postprocessed using an imaging processing software (VirtualDub v1.9.10) and dynamic contact angle measurements

Table 1 Measurements of dynamic contact angles of slug flows in Fig. 6

Figure 6	Surface wettability	Static contract angle (θ_s)	Advancing dynamic contact angle ($\theta_{d,\mathrm{adv}}$)	Receding dynamic contact angle ($\theta_{d,\mathrm{rec}}$)	$\theta_s - \theta_{d,\mathrm{adv}}$	$\theta_s - \theta_{d,\mathrm{rec}}$
(a)	Super-hydrophobic	150°	7°	47°	143°	103°
(b)	Hydrophobic	105°	22°	46°	83°	59°
(c)	Hydrophilic	60°	25°	46°	35°	14°
(d)	Super-hydrophilic	25°	23°	40°	2°	−15°

where $\theta_{d,\mathrm{adv}} = \theta_{d,\mathrm{advancing}}$ and $\theta_{d,\mathrm{rec}} = \theta_{d,\mathrm{receding}}$

Dynamic contact angles are measured, on images postprocessed in VirtualDub software, using National Instruments Vision software. The interfaces are determined manually using various background contrasting functions available in an image processing software (National Instrument Vision™). Angles measured are within uncertainty of ±5°

are carried out using National Instruments Vision™ software. Table 1 summarizes the measured dynamic contact angles of slug flows in Fig. 6, and the deviation from static contact angles which are measured by sessile-drop method which is described in Sect. 2.1. For (super) hydrophilic microchannels, the advancing interface is similar to the receding interface in shape. The measured dynamic contact angles of hydrophilic microchannels are within the similar range of static contact angles. With decreasing wettabiltiy from superhydrophilic to superhydrophobic, dynamic contact angle deviation from its static value ($\theta_s - \theta_d$) changes from −15° to 143°. The dynamic contact angle deviates drastically from static contact angle as surface energy decreases (hydrophobicity increases). As was found by Qian et al. (2003) and Weiqing and Weinan (2007), Young's stress in the contact line region is dominant even in cases when the dynamic contact angle deviates only slightly from the static contact angle (denoted by $\theta_s - \theta_d$). The difference of dynamic contact angles between advancing and receding fronts ($\Delta\theta_d = \theta_{d,\mathrm{advancing}} - \theta_{d,\mathrm{reciding}}$) is also significant in hydrophobic and superhydrophobic cases. Value of $\Delta\theta_d$ varies from 30° to 10° for superhydrophobic surfaces to superhydrophilic surfaces.

3.2 Two-phase flow resistance versus surface wettability

Flow resistance caused by shear stress and Young's stress in microchannel two-phase flow is a parameter of prime interest to determine the flow conditions. Figure 7 indicates the variation of average two-phase flow resistance per unit length for two-phase flow in microchannels ($D_h = 700$ μm) against surface wettability (static contact angle) for various liquid volumetric fractions (α_L). Shape of markers is used to represent geometry of the channel in Fig. 7.

For given value of α_L and wettability, two-phase flow resistance in circular channels is higher than that in square channels. While the liquid volumetric fraction (α_L) increases, the two-phase flow resistance also increases due to higher shear stress experienced on account of higher flow velocities.
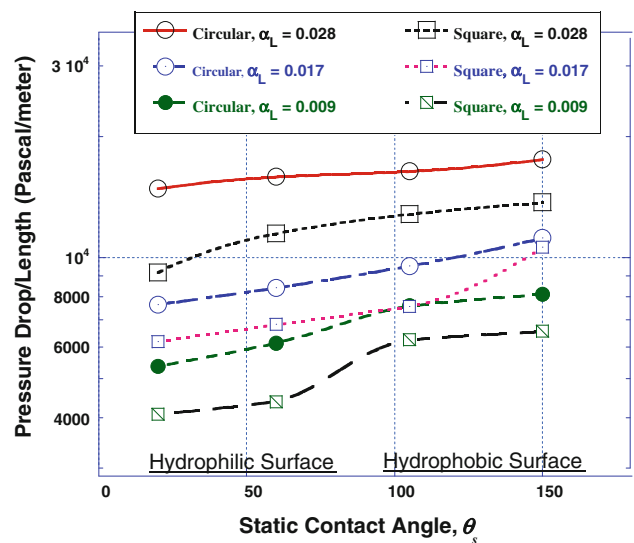

Fig. 7 Two-phase flow resistance per unit length versus surface wettability for flows at various liquid volumetric fractions, α_L ($D_h = 700$ μm and Length = 127 mm); α_L of 0.028 ($Q_L = 4.6 \times 10^{-8}$ m³/s and $Q_G = 1.6 \times 10^{-6}$ m³/s), α_L of 0.017 ($Q_L = 2.4 \times 10^{-8}$ m³/s and $Q_G = 1.4 \times 10^{-6}$ m³/s), and α_L of 0.009 ($Q_L = 1.2 \times 10^{-8}$ m³/s and $Q_G = 1.7 \times 10^{-6}$ m³/s)

In order to estimate the capillary effect (Young's stress) on the flow resistance, we may apply the well-known modified Young's equation at the interfaces of bubbles in slug flows (Fig. 5);

$$\Delta P = \frac{4\sigma\cos\theta_d}{D_h} \qquad (2)$$

where ΔP is the pressure differential across the interface, σ is the surface tension of water, and D_h is the hydraulic diameter of microchannel. When the direction of capillary force is considered, the summation of pressure drop (ΔP_{sum}) related to the single bubble (Fig. 5) can be expressed as;

$$\Delta P_{\mathrm{sum}} = \frac{4\sigma\left(\cos\theta_{d,\mathrm{advancing}} - \cos\theta_{d,\mathrm{receding}}\right)}{D_h} \qquad (3)$$

ΔP_{sum} can be the maximum flow resistance induced by capillary force if there is no liquid film between bubble and

Table 2 Flow resistance induced by capillary force of individual slug in various surface wettabilities microchannels

Figure 6	Surface wettability	Advancing dynamic contact angle ($\theta_{d,\mathrm{adv}}$)	Receding dynamic contact angle ($\theta_{d,\mathrm{rec}}$)	Diff = $\cos(\theta_{d,\mathrm{adv}}) - \cos(\theta_{d,\mathrm{rec}})$	Dynamic capillary resistance for individual slug = $\frac{4\sigma*\mathrm{Diff}}{D_h}$ (Pascal)
(a)	Super-hydrophobic	7°	47°	0.31	64.5
(b)	Hydrophobic	22°	46°	0.23	48.1
(c)	Hydrophilic	25°	46°	0.21	41.4
(d)	Super-hydrophilic	23°	40°	0.15	33.5

where $\theta_{d,\mathrm{adv}} = \theta_{d,\mathrm{advancing}}$ and $\theta_{d,\mathrm{rec}} = \theta_{d,\mathrm{receding}}$

Dynamic contact angles are measured, on images postprocessed in Virtual Dub software, using National Instruments Vision software. The interfaces are determined manually using various background contrasting functions available in an image processing software (National Instrument Vision[TM]). Angles measured are within uncertainty of ±5°

channel wall. However, depending on wettability of channel wall, the liquid film can exist and its thickness may increase when the surface energy increase (wettability increases). The contribution of capillary force by each completely snapped-off slug to two-phase flow resistance is highlighted with surface wettability in Table 2. As evident in this table, the capillary resistance calculated using Eq. 3 increases as the surface wettability decreases. This is identical trend to the results of pressure drop increase as the surface wettability decreases in Fig. 7. When the contact angle difference between the static and the dynamic ($\theta_s - \theta_d$) scenario increases, capillary resistance experienced by slug at advancing and receding fronts increases significantly. Then, the capillary resistance lastly results in the pressure drop of microchannel slug flow. Ratulowski and Chang (1990) proposed an expression for the pressure drop, assuming that the pressure drop is the sum of the pressure drops across bubbles and liquid slugs.

3.3 Two-phase flow resistance versus geometry of channels and liquid film

In order to observe the effect of channel geometry on flow resistance, the pressure drop of circular channels is compared with square channels' at the same liquid volumetric fractions, α_L in Fig. 7. The pressure drop of circular channel flows of our experimental conditions is always higher than that of square channel flows in the whole range of liquid volumetric fractions (α_L) and for all channel surface wettability conditions even though we consider the superficial velocity ($U_L = Q_L/A$, A is the cross-sectional area of channel) of circular channels is 21% faster than the superficial velocity of square channels. As discussed in Sect. 3.2, the flow resistance is affected by the capillary resistance which is induced by the dynamic contact angle difference at the interfaces of bubbles. The flow resistance is also proportional to the number of bubbles in the slug microchannel flow. If there are more bubbles in the slug
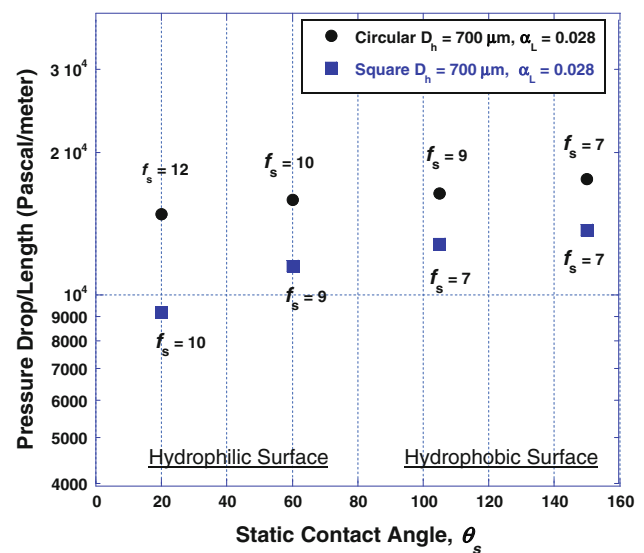

Fig. 8 Two-phase flow resistance in 700 μm microchannels of various surface wettabilities (static contact angles) and geometries at the same liquid volumetric fraction, $\alpha_L = 0.028$ ($Q_L = 4.6 \times 10^{-8}$ m³/s and $Q_G = 1.6 \times 10^{-6}$ m³/s). Uncertainty in pressure measurement is ±250 Pa. Average deviation of the reported slug frequency values is observed to be within 7% to 29%

flows, more capillary resistance contributes to the total pressure drop. Therefore, the slug frequency (f_s) is measured by counting the number of completely snapped-off slugs observed per second of slug flow. For the same flow conditions of $\alpha_L = 0.028$ and surface wettability, slug frequency observed in the square microchannel is lesser than the circular channel's (Fig. 8). This observed phenomenon can be attributed to the corner effects encountered in square channel geometries. At the sharp corners of square channel, the liquid is filled and stays by capillarity when the corner satisfies the Concus–Finn condition: $\theta_s < \pi/2 - \alpha$ where α is the half-angle of corner (Concus and Finn 1974). It is expected that the liquid thickness at the corners is thicker than the liquid film thickness at the wall of circular channels. The resulting capillary force at

the corners of square channel is smaller than capillary force of circular channels. As a result, the pressure drop of circular channel flow is higher than that of square channel flows. The hydrophilic and superhydrophilic channels satisfy the Concus–Finn condition, and then it is expected that liquid is stayed in the corner during experiments.

Furthermore, the slug frequency (f_s) observed in superhydrophilic channel flow is higher than that observed in superhydrophobic channels. Even though there are more bubbles generated in hydrophilic channel flows than hydrophobic channel flows, the flow resistance of hydrophilic channel flows is less than that of hydrophobic channel flows. It implies that the capillary resistance induced by the bubble of hydrophilic channel is less than hydrophobic channel case. Furthermore, the flow resistance of slug flow can be accounted by the wettability of channel. The results in Fig. 8 also imply that the actual capillary resistance induced by a single bubble in hydrophilic slug flow is less than Laplace–Young's estimation using dynamic contact angles (Eq. 3). It may be explained by the liquid film which can be formed between bubble and channel wall. The hydrophilic channel may form the thicker liquid film than the hydrophobic wall due to its high surface energy.

Experiments were carried out in order to estimate indirectly the thickness of liquid film which is formed between bubble and channel wall during slug flow in microchannels of various surface wettabilities. The indirect liquid film measurement is carried out using following procedure; (a) a known mass of water is infused into the circular microchannels of various diameters using gas-tight precision syringe followed by supply of humidified air at experimental flow rate conditions. (b) The mass of water drained off the tube is estimated by measuring the Petri dish in the precision microbalance (make and model: A&D GH-252, Range: 101/250 g, resolution: 0.01/0.1 mg,) before and after liquid water drain off. (c) Mass of liquid water retained in the microchannel is obtained by the difference between total mass of liquid water injected and mass of liquid drained. (d) Assuming that liquid water retained in the microchannel remains as liquid circular film of uniform thickness along the channel length, thickness of the liquid film (δ) is calculated. The liquid film values calculated, using the above mass balance procedure, are found to be within standard average deviation of 25%.

Figure 9 represents variation of calculated thickness of liquid film with surface wettability for various microchannels. The thickness of liquid (water) film in superhydrophilic channels ($\delta = 12 \, \mu m$) is an order of magnitude higher when compared to that in superhydrophobic channels ($\delta = 2 \, \mu m$). From Fig. 9, it can be ascertained that there exists liquid film for hydrophilic channels whose thickness increases with increase of surface wettability. In
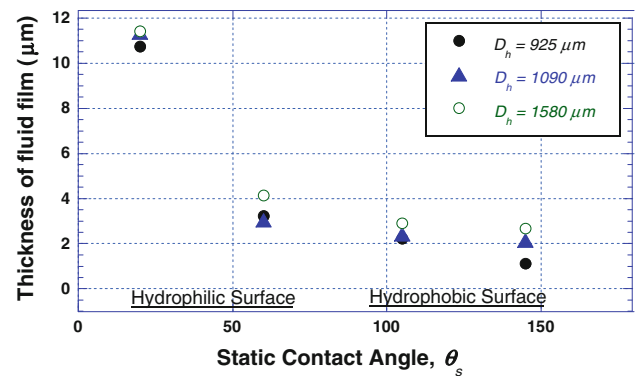

Fig. 9 Thickness of liquid film against surface wettability (static contact angles) for various hydraulic diameter (D_h) circular channels with 127 mm length. Estimated fluid film thickness values are found to be within standard average deviation of 25%

superhydrophilic surfaces because of thick fluid film, flow is more of "bubbly" flow which is less affected by wall (minimal capillary effect).

A requirement for Laplace–Young equation (Eqs. 2, 3) is the three-phase (liquid–gas-solid) contact line. But when surface energy (wettability) increases, as evident in Figs. 5 and 9 a liquid film exists thereby resulting in no dry-solid surface exists inside of a single bubble (Fig. 5). Therefore, the capillary resistance decreases in slug flows of hydrophilic microchannles where the liquid film forms between bubble and solid channel wall. As the thickness of liquid film increases, the capillary effect decreases. However, for (super) hydrophobic surfaces, thinner (or no) liquid film facilitates three-phase contact (liquid, air, and dry surface) at the interface. Hence, the pressure drops of (super) hydrophobic channels are affected by capillary force formed at the interfaces of advancing and receding. It results in the higher pressure drop due to the higher capillary effect nonetheless less slug frequency in the hydrophobic slug microchannel flows.

4 Conclusion

In this present work, we aimed to provide data allowing understanding the role of surface wettability on the two-phase flow characteristics in isothermal horizontal microchannels. Two-phase slug flow in microchannels is experimentally characterized using the two-phase pressure drops and flow visualization. It was found that the surface wettability is an important parameter to affect the pressure drop of slug flow in microchannel. The pressure drop of hydrophobic channel is mainly governed by the capillary resistance which is induced by the dynamic contact angle difference at the interfaces of bubble in slug flow. However, the influence of capillary resistance on pressure drop of hydrophilic channel flow is relatively small. It is

explained by the effect of liquid film formed between bubble and channel wall with assumption of that the thicker liquid film diminishes more capillary resistance. The comparison between the slug flows of different channel geometries resulted in the circular channel is generating more bubble in slug flow than the square channel slug flow.

References

Allen JS, Son SY (2007) High speed microscopic visualization of isothermal gas-liquid flow in microchannels. In: 18th International symposium on transport phenomena, Daejon, Korea, pp 2037–2042

Barajas AB, Panton RL (1994) Effects of contact angle on two-phase flow in capillary tubes. Int J Multiphase Flow 19:337–346

Bi QC, Zhao TS (2001) Taylor bubbles in miniaturized circular and noncircular channels. Int J Multiphase Flow 27:561–570

Concus P, Finn R (1974) On capillary free surfaces in the absence of gravity. Acta Mathematica 132:177–198

Cubaud T, Ho CM (2004) Transport of bubbles in square microchannels. Phys Fluids 16:4575–4585

Damianides CA, Westwater JW (1988) Two-phase flow patterns in a compact heat exchanger and in small tubes. In: Proceedings of 2nd UK national conference on heat transfer, p 1257

Graska ML (1986) Effects of fluid surface tension and tube diameter on horizontal two-phase flow in small diameter tubes. M.S. Thesis, University of Illinois at Urbana-Champaign, IL

Ichikawa N, Chung PM, Matsumoto S, Matsumoto JI, Takada N (2005) Interface motion driven by capillary action in circular and rectangular microchannel. Microscale Thermophys Eng 9:237–254

Jeong HJ, Kim DK, Lee SB, Kwon SH, Kadono K (2001) Preparation of water-repellent glass by sol–gel process using perfluoroalkylsilane and tetraethoxysilane. J Colloid Interface Sci 235:130–134

Lee CY, Lee SY (2008a) Pressure drop of two-phase plug flow in round mini-channels: influence of surface wettability. Exp Thermal Fluid Sci 32:1716–1722

Lee CY, Lee SY (2008b) Influence of surface wettability on transition of two-phase flow pattern in round mini-channels. Int J Multiphase Flow 34:706–711

Qian T, Wang XP, Sheng P (2003) Molecular scale contact line hydrodynamics of immiscible flows. Phys Rev E Stat Nonlinear Soft Matter Phys 68:163061–1630615

Ratulowski J, Chang HC (1990) Marangoni effects of trace impurities on the motion of long gas-bubbles in capillaries. J Fluid Mech 210:303–328

Son SY, Allen JS (2003) Observation of low bond number two-phase flow regime transition from slug to annular wavy flow in a microchannel. ICMM 1:473–477

Son SY, Allen JS (2004) Visualization of wettability effects on microchannel two-phase flow resistance. J of Heat Transfer 126:498–499

Son SY, Allen JS (2005) Visualization and predictive modeling of two-phase flow regime transition with application towards water management in the gas-flow channels of PEM fuel cells, 2005 ASME international mechanical engineering congress and exposition, IMECE2005-82422, Orlando, Florida, 5–11 Nov

Suo M, Griffith P (1964) Two-phase flow in capillary tubes. Trans ASME J Basic Eng 86:576–582

Tadanaga K, Morinaga J, Minami T (2000) Formation of Superhydrophobic—Superhydrophilic pattern on flowerlike alumina thin film by the sol–gel method. J Sol–Gel Sci Technol 19:211–214

Weiqing R, Weinan E (2007) Boundary conditions for the moving contact line problem. Phys Fluids 19:022101–022115. doi: 10.1063/1.2646754